Title

Microbial community dynamics and coexistence in a sulfide-driven phototrophic bloom

Authors

Srijak Bhatnagar†, Elise S. Cowley†, Sebastian H. Kopf, Sherlynette Pérez Castro, Sean Kearney, Scott C. Dawson, Kurt Hanselmann, S. Emil Ruff *

† Denotes equal contribution

* Corresponding author

Author Affiliations

SB: Geomicrobiology Group, University of Calgary, Alberta, Canada; srijak.bhatnagar@ucalgary.ca

ESC: Medical Scientist Training Program, School of Medicine and Public Health, University of Wisconsin-Madison, Madison, WI, USA; ecowley@wisc.edu

SHK: Department of Geological Sciences, University of Colorado, Boulder, CO, USA; sebastian.kopf@colorado.edu

SPC: Ecosystems Center/Bay Paul Center, Marine Biological Laboratory, Woods Hole, MA, USA; sperezcastro@mbl.edu

SK: Department of Biological Engineering, Massachusetts Institute of Technology, Cambridge, MA, USA; skearney@mit.edu

SCD: Department of Microbiology and Molecular Genetics, University of California Davis, CA, USA; scdawson@ucdavis.edu

KH: Department of Earth Sciences, ETH-Z, Zürich, CH; kurt.hanselmann@erdw.ethz.ch

SER: Ecosystems Center/Bay Paul Center, Marine Biological Laboratory, Woods Hole, MA, USA; eruff@mbl.edu

Keywords

Microbial succession, Green sulfur bacteria, Prosthecochloris, microbial bloom, brackish coastal ecosystem, anoxygenic phototrophy, Microviridae, virus, CRISPR-Cas, resilience

Abstract

Phototrophic microbial mats commonly contain multiple phototrophic lineages that coexist based on their light, oxygen and nutrient preferences. Here we show that similar coexistence patterns and ecological niches can occur in suspended phototrophic blooms of an organic-rich estuary. The water column showed steep gradients of oxygen, pH, sulfate, sulfide, and salinity. The upper part of the bloom was dominated by aerobic phototrophic *Cyanobacteria*, the middle and lower parts were dominated by anoxygenic purple sulfur bacteria (*Chromatiales*) and green sulfur bacteria (*Chlorobiales*), respectively. We found multiple uncultured phototrophic lineages and present metagenome-assembled genomes of two uncultured organisms within the *Chlorobiales*. Apparently, those *Chlorobiales* populations were affected by *Microviridae* viruses. We suggest a cryptic sulfur cycle within the bloom in which elemental sulfur produced by phototrophs is reduced to sulfide by *Desulfuromonas sp*. These findings improve our understanding of the ecology and ecophysiology of phototrophic blooms and their impact on biogeochemical cycles.

Introduction

Estuarine and coastal water bodies are dynamic and ubiquitous ecosystems that are often characterized by the mixing of terrestrial freshwater and ocean saltwater. Brackish habitats can have striking physical and chemical characteristics that differ from both fresh and saltwater ecosystems (McLusky and Elliott, 2004; Moore, 1999). Brackish ecosystems are very diverse and support large microbial and macrobial communities (McLusky and Elliott, 2004). Estuaries also provide crucial ecosystem services, the most salient of which is trapping and filtering terrestrial runoffs and pollutants before they enter the oceans (Jay et al., 2007; Nelson and Zavaleta, 2012; Pant and Reddy, 2001).

Estuaries harbor abundant and diverse microbial communities that participate in the cycling of carbon, nitrogen, sulfur, and phosphorus. These communities fix carbon dioxide through photosynthesis or chemosynthesis (Boschker et al., 2014; Ritchie and Johnson, 2012; Waidner and Kirchman, 2005). Additionally, carbon introduced as

organic matter from the oceans or land can be remineralized by heterotrophic microbial communities (Moran et al., 2000; Peduzzi and Herndl, 1991; Smith and Hollibaugh, 1993). This decomposition can deposit sulfide in sediments (Capone and Kiene, 1988). Further, sulfate brought into estuaries by ocean waters can be utilized by sulfate reducers, which convert sulfate into elemental sulfur or sulfide (Capone and Kiene, 1988; Purdy et al., 2002). The combination of sulfate introduced by ocean water and sulfide released from decomposition in the sediments is part of the chemocline of the brackish water column (Zopfi et al., 2001). Additionally, estuaries and coastal marshes often exhibit a halocline and the depletion of oxygen in the water column can create an oxycline (Lee et al., 2015; Long, 1976). These gradients can produce habitats and niches that influence microbial community structure at different depths and conversely the microbial community can respond to these gradients (Jørgensen and Revsbech, 1983; Møller et al., 1985; Wimpenny et al., 1982).

The physicochemical properties of estuaries fluctuate frequently and rapidly as a result of many factors, for example, tidal cycles, weather patterns, and seasonal cycles (Allen et al., 1980; Badr et al., 2008; Garvine, 1985; Haas, 1977; Maie et al., 2006; Simpson et al., 1990). Such disturbances can bring about noticeable changes in the microbial community structure of the ecosystem, including blooms or declines in the populations of one or more members of the microbial community, as well as changes in the richness and evenness of the community (Bernhard et al., 2005; Henriques et al., 2006; Lv et al., 2016; Muylaert et al., 2000; Zaikova et al., 2010).

Trunk River in Woods Hole, MA is a brackish ecosystem, on the coast of Vineyard Sound (N 41.535236, W -70.641298). Near the mouth, Trunk River forms a shallow lagoon where freshwater mixes with seawater. Storms, tides, and run-off introduce large amounts of biomass to the pond forming thick layers of decaying seagrass and other organic matter. The pond has a distinct sulfidic odor that emanates from the water and gases bubble up from the sediment. Episodically, strikingly yellow microbial blooms can be observed just below the water surface (see Figure 1, S1) that typically disappear again within days to weeks. These transient blooms were observed to occur in natural depressions in the decaying organic matter and anecdotally seemed to be initiated by

physical disturbance events, potentially from storms, tidal extremes, human activity, or animals. Given this visually striking natural ecological progression, we set out to test whether physical disturbance alone could trigger the blooms.

To understand the mechanisms of bloom development, we thus mimicked such disturbances of the brackish ecosystem by creating artificial depressions in the decaying organic matter, and monitored the microbial community response and population dynamics, as well as investigated ecological niches of the key populations. Based on previous observations, we hypothesized that i) the disturbance would cause a sulfide-driven phototrophic bloom ii) due to its rapid development the bloom would be largely dominated by very few populations and iii) sharp photo-/ and physicochemical gradients would establish that cause narrow habitats and niches. We discuss the resulting reproducible ecological succession and provide insights into the habitats, niches, and resilience of such widespread ecosystems. Our findings contribute to the understanding of the ecological processes and dynamics that shape phototrophic blooms, which are a naturally occurring phenomenon in many ecosystems.

Results

Visual Observations

At the first sampling time point (2 days post-disturbance), no difference was observed in the water column or in the samples collected from different depths. Two days later (time point 2, 4 days post-disturbance), a faint pink layer was observed in the water column, and faint shades of yellow in samples from the 25 cm depth (Figure S2). At the next sampling time point (time point 3; 5 days post-disturbance), we observed a bright yellow suspension below the water surface (Figure 1). Of the samples collected at this time point, the samples from 25 cm depth were most distinctly yellow (Figure S2). The yellow color of the suspension intensified by time point 4 (7 days post-disturbance). No remarkable visual changes in the system were observed for the subsequent three time points (time points 5, 6, and 7). During these three time points, the yellow suspension only slightly changed. At time point 8 (16 days post-disturbance), the holes had partially collapsed, the water was much clearer and the 25-cm samples showed a reduction in

the intensity of the yellow color (Figure S2). We found a green layer at the bottom of each hole, seemingly from sedimented GSB. It has to be noted that the opacity of the samples was higher at the first two timepoints than at the following timepoints. Especially at timepoint 1 the suspension was beige and very opaque, while later on the suspension became more yellow, but also more translucent (Figure S2).

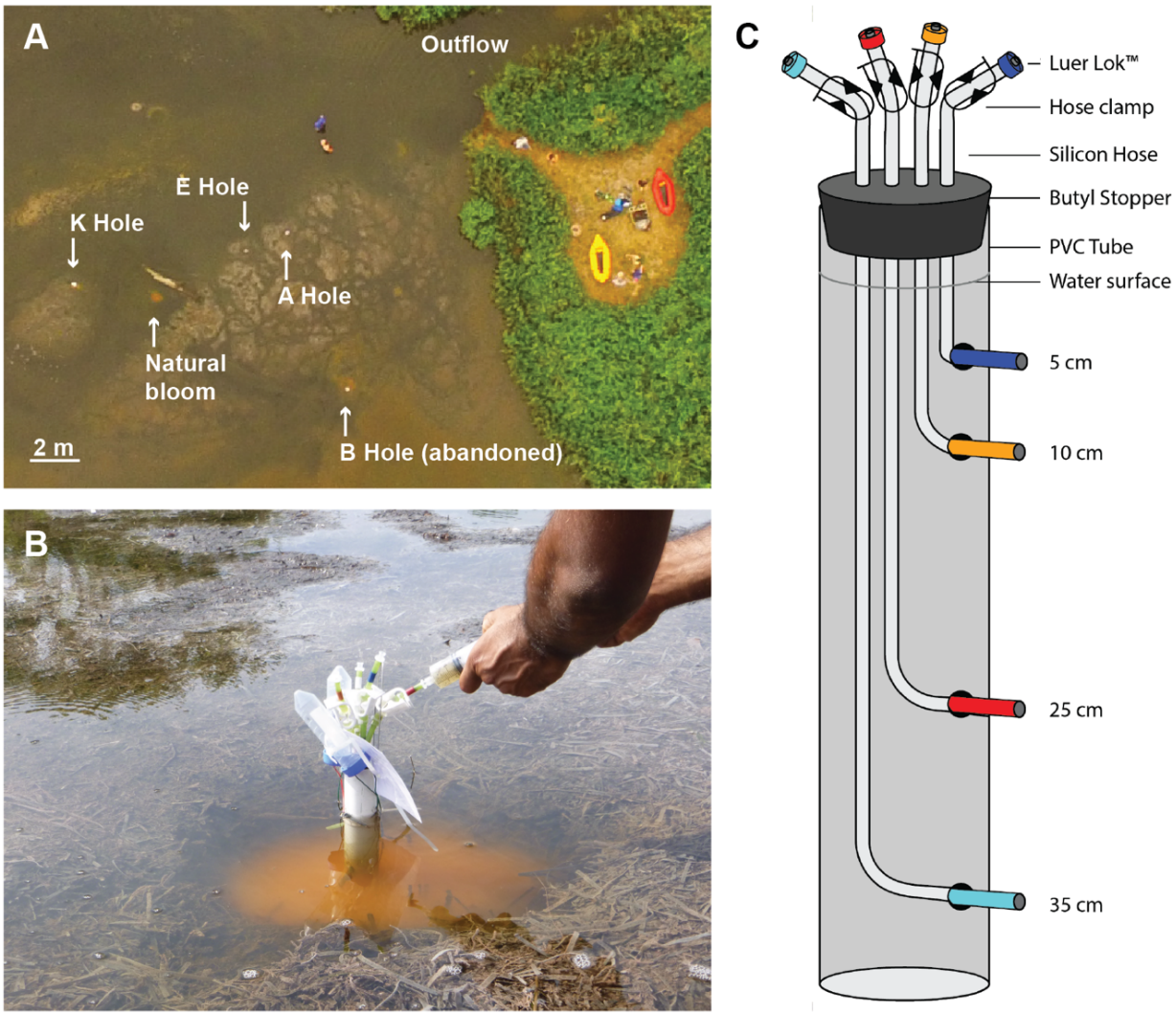

Figure 1: Sampling sites. A. Aerial view of experimental sites (A, E, and K) in the Trunk river lagoon. The water enters the lagoon from the right and exits to the sea through a channel marked outlet. **B.** View of a **LEMON** (**L**ong-term **E**nvironmental **MON**itoring) sampling device during sample collection on time point 3; 5 days post-disturbance. **C.** Schematic of the LEMON.

Physicochemistry of the water column

Within the first three days the pH decreased between one and two units in all layers, with lowest values present in the deepest layer (Figure 2). Over the 15-day sampling period, pH showed more variation in the two upper layers than in the two deeper layers were it was very constant at values between 6 and 6.3. Throughout the experiment the water column in all three experiments showed a stable halocline with brackish water (5 ‰ salinity) at the water surface and saltwater (30 ‰) at 35 cm depth (Figure 2). Salinity increased with depth and was 12 ‰ and 23 ‰ at 10 cm and 25 cm, respectively. Major ions also reflect this trend (e.g. calcium, potassium in Figure S5). The dissolved oxygen (DO) concentrations showed a stable oxycline between 10 and 25 cm. Above 10 cm, DO was always higher than 20 % (36±17 %) and below that DO was always below 20 % (9±9 %). The oxygen concentration slowly decreased in the upper two layers during the first half of the experiment, but recovered again to the original values towards the end of the experiment. At 5 and 10 cm, DO was approximately 41 % and 30 %, respectively (Figure 2). At 25 and 35 cm, the average DO measurements were ≈ 12 % and 5%, respectively. The sulfate concentrations in the water column decreased along the depth gradient, with the highest sulfate concentration at 5 cm (≈ 2 mM) and the lowest at 25 cm (≈ 0.2 mM) (Figure 2). In contrast, the sulfide concentrations were lowest at 5 cm (Figure 2F). Interestingly, the greatest sulfide concentration was measured at 10 cm depth peaking at over 1 mM towards the end of the experiment. Below 10 cm, sulfide concentration was still high, but declined to 0.75 mM ± 0.22 at 25 cm and 0.5 mM ± 0.17 at 35 cm. The normalized biomass measured for the 5 cm samples throughout the sampling period was nearly zero (Figure 2). At 10 cm, 25 cm, and 35 cm, the normalized biomass measured was approximately, 0.2 mg/mL, 0.3 mg/mL, and 0.2 mg/mL, respectively. For details concerning iron (Fe(II), Fe(III), total Fe), nitrate, calcium, potassium, ammonium and acetate refer to Supplementary Results and Figure S5.

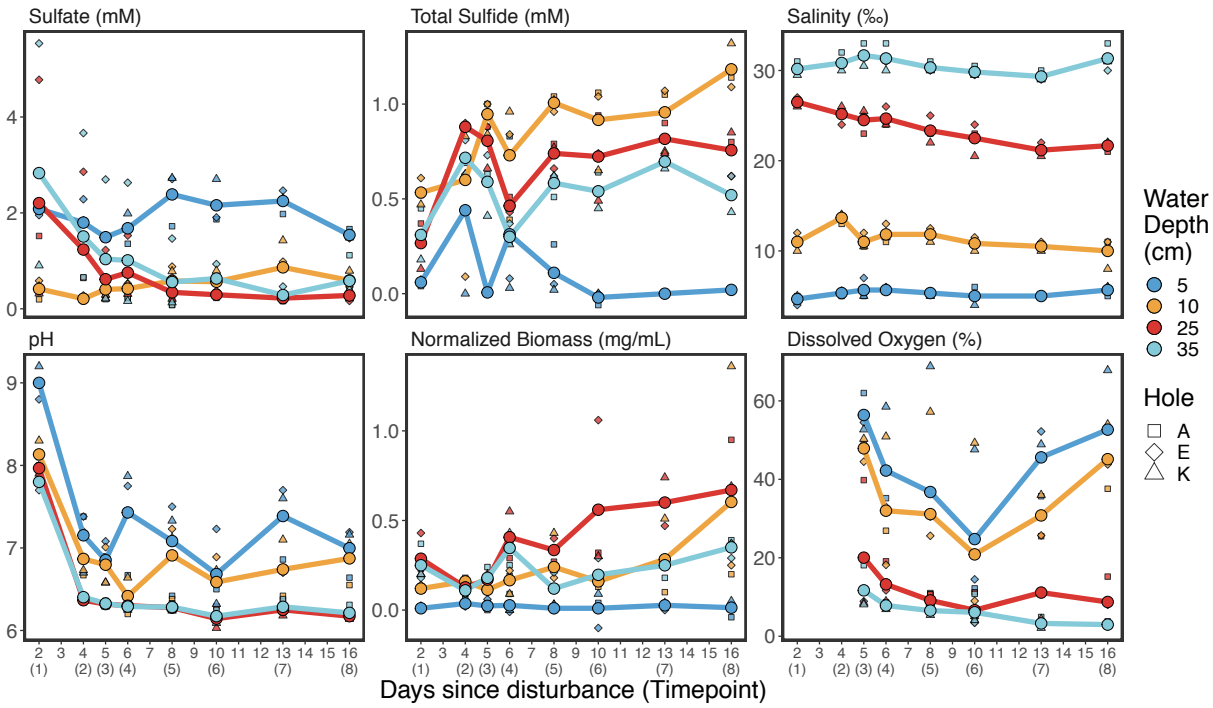

Figure 2: **Physicochemistry**. The physicochemical measurements of the sampling sites. Salinity (parts per thousand). The x-axis shows days since disturbance and the y-axis the respective units. For further parameters (Fe (II); Fe (III); Total Fe, nitrate) refer to SI.

Spectral Absorbance of Phototrophic Community

We measured absorbance spectra from filters of samples from A, E and K experiments (Figure S3) and compared the spectra to those of representative cultured species of the most abundant phototrophic genera from the literature (Borrego et al., 1999; Caumette et al., 1997; Oren, 2011; Srinivas et al., 2009; Stomp et al., 2008). All absorbance spectra were normalized to the respective highest peak (Figure 3). Our results show that pigments belonging to PSB were prominent in the upper layer of the bloom (orange spectra), while GSB pigments dominated the lower layer of the bloom (red line). Pigments characteristic for *Cyanobacteria* were less abundant at peak bloom and increased relatively at the end of the experiment. Pigments of all major phototrophs were detected throughout the experiment. The spectral results suggest the coexistence of multiple phototrophs over the entire duration of the experiment.

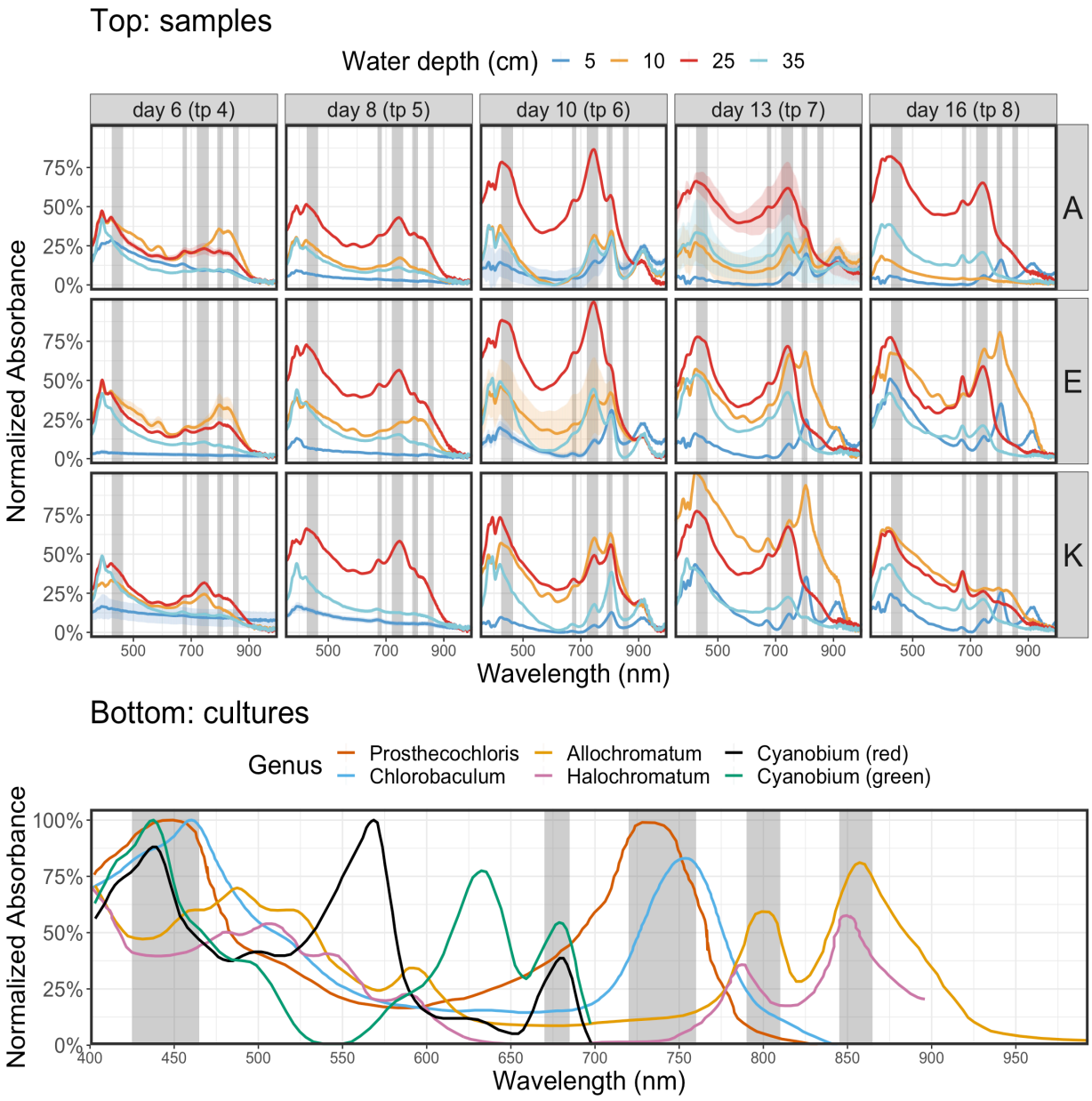

Figure 3: **Spectral Absorbance**. Sample spectra show averages of at least three replicates per sample. Color bands in the sample data indicate one standard deviation (bands are mostly smaller than center line). Gray vertical bands indicate major absorbance peaks of the *Prosthecochloris* and *Chlorobaculum* group (720-760 nm) and the *Allochromatium* and *Halochromatium* group (790-810 nm and 845-865 nm) highlighting the transient appearance and likely dominance of these phototrophs over the course of the experiments. Also indicated is the general phototroph absorbance band in the 425-465 nm window. Cyanobacterial groups (red and green) have distinct absorbance peaks in the 500-700 nm range that are not prominent in the sample spectra except for the characteristic 670-685 nm peak (also highlighted in gray) reflecting the presence but likely smaller role of these taxa during the experiment.

Microbial Community Structure and Taxonomic Composition

At the beginning of the experiment, the microbial diversity was high in all four water depths and very similar across replicate ecosystems. Alpha diversity rapidly decreased with the onset of the bloom, and within two days the communities in the four depth layers substantially changed (Figure 4, 5, S6, S7). The number of observed amplicon sequence variants (ASV), as well as estimated richness, Shannon entropy, and Inverse Simpson diversity significantly decreased between the surface water and the water at a depth of 10 cm and 25 cm (Figure 4; p=0.001). This change is most striking in the case of Inverse Simpson diversity, a measure for evenness. In just one day, evenness dropped in both 10 cm and 25 cm water depth by over one order of magnitude to low single digit values (Figure 4; Table S1). This means the community was extremely dominated by one ASV (a pure culture has an Inverse Simpson diversity of 1).

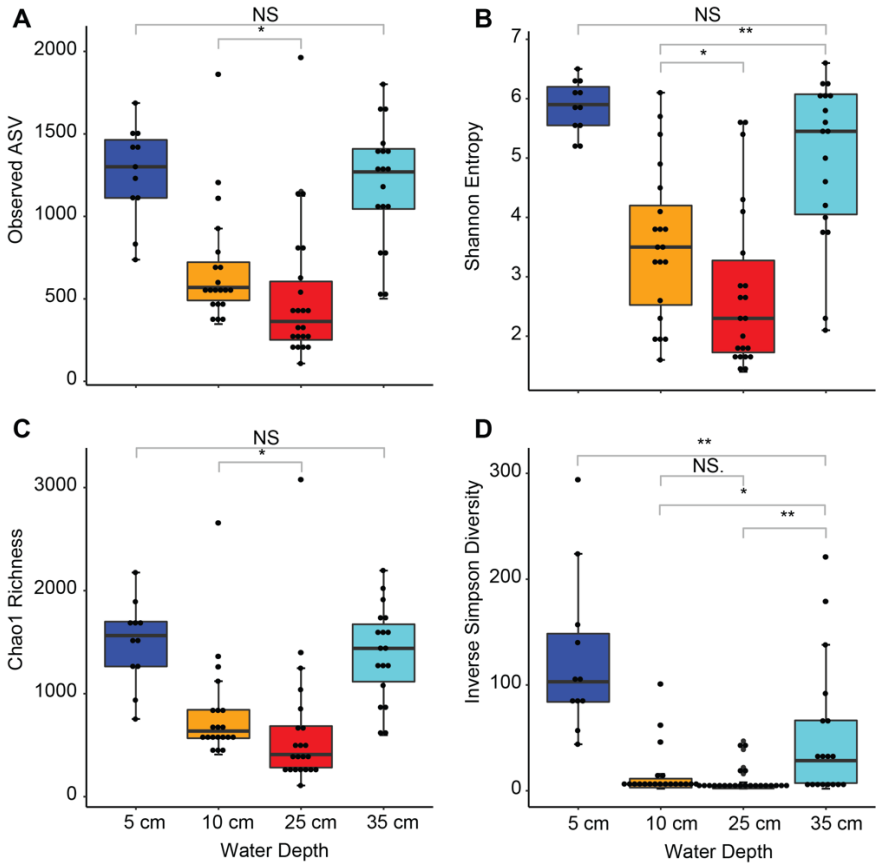

Figure 4: Alpha diversity. Diversity Indices of all samples grouped by depth. Pairwise comparisons with low significance levels are shown (NS, *: p<0.1, **: p<0.01). All pairwise comparisons that are not shown were highly significant (***: p<0.001), e.g. panel A 5 cm vs 10 cm.

The rapid and profound change of community structure is corroborated by a high turnover of ASV between the layers and timepoints, as shown by non-metric multidimensional scaling (Figure 5, S7). The top layer is well separated from the deeper layers. The communities at 25 cm water depth experienced the largest turnover, i.e. change in community structure, as shown in the ordination (Figure 5). The more distant two points are on the ordination plot the less similar are the underlying communities. Interestingly, the communities of all three deep layers (15 – 35 cm) had a similar community structure at the beginning of the experiment and then seemed to converge again at the end, yet at a different part of the ordination plot. This pattern on the ordination plot indicates that the bloom shifted the microbial communities to an alternative stable state.

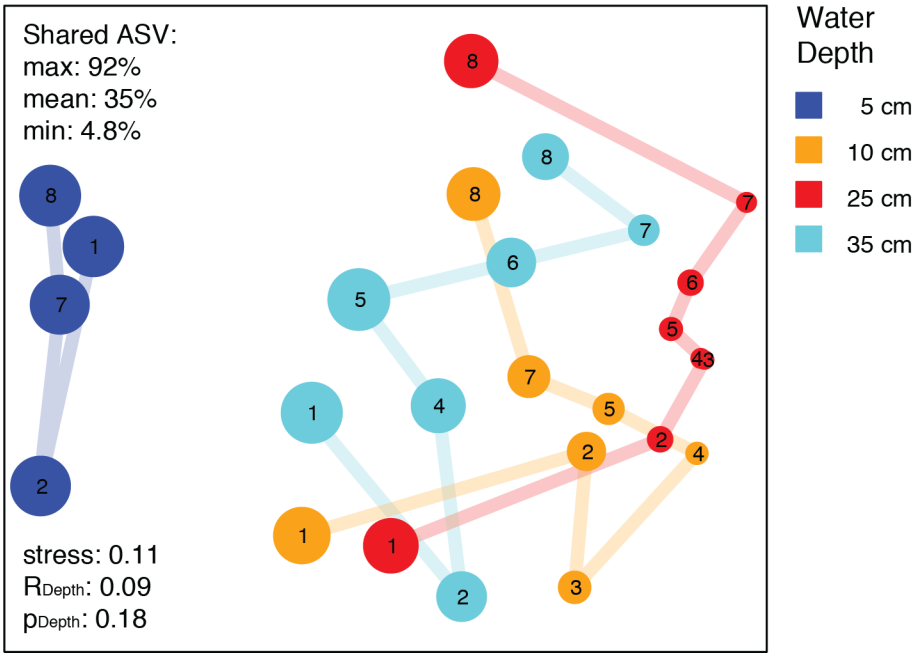

Figure 5: Microbial Community Turnover. Circle size represents average Shannon Diversity across three replicate holes. Sampling time points are indicated as numbers. The ordination shows that communities in 15-35 cm water depth are very different from those in the top layer. The trajectories indicate that layer 2 and 3 underwent the most substantial changes in community structure. The community at 25 cm depth had a striking loss in diversity during the experiment, yet seemed to have recovered at the last time point. Holes were very similar (see SI Figure S4) and were averaged for clarity. ASV: Amplicon Sequence Variant. Depth is not a significant indicator for community structure using replicate averages, however in each hole the communities in the different layers are overlapping but different (see Figure S4).

The taxonomic composition was assessed at all phylogenetic levels (Figure 6, S8). We observed a total of 73 bacterial phyla. The surface community (5 cm) remained relatively unchanged throughout the experiment and was dominated by *Proteobacteria*, *Chlorobi*, *Cyanobacteria* and *Actinobacteria*. The communities in the deeper layers were more dynamic, being dominated by *Bacteroidetes*, *Proteobacteria*, *Firmicutes*, and *Chloroflexi*. In general, taxonomic diversity was highest in the deepest layer (35 cm). The profound change in diversity was accompanied by a change in composition. Within a few days, there was a substantial increase in the abundance of *Chlorobi*, which comprised more than 75% of the community at that time. This increase persisted for nine days, but levelled off at the end of the experiment. The datasets of all layers and timepoints were dominated by ASVs affiliating with phototrophic organisms, as shown by relative sequence abundances on genus level (Figure 6A). Some phototrophs occurred in all layers at similar relative sequence abundances, such as *Halochromatium* and "*Candidatus* Chloroploca". The stable surface layer harbored *Cyanobium* and "*Candidatus* Aquiluna", which decreased in the deeper layers. The upper layer of the bloom showed an increased relative sequence abundance of *Allochromatium,* the lower bloom layer was dominated by *Prosthecochloris* and *Chlorobaculum* (Figure S10). Interestingly, almost all *Prosthecochloris* affiliated reads belonged to a single sequence variant, while ASV diversity affiliated with the closely related *Chlorobaculum* increased over time (Figure 6B, S9).

The relative sequence abundance of *Chlorobiales* noticeably changed at 25 cm depth, where the yellow microbial bloom was visually observed. *Chlorobiales* ASVs accounted for >25 % of reads in our dataset. To identify the phylogeny of ASV affiliating with *Chlorobiales*, we placed the representative sequence of each ASV on a reference tree of known *Chlorobiales*. The most abundant *Chlorobiales* ASV (ASV_1) affiliated with the genus *Prosthecochloris*, and specifically in the monophyletic clade of *Prosthecochloris vibrioformis* (Figure S11), followed by an ASV (ASV_2) affiliating with *Chlorobaculum*. Together, these two ASVs account for >97 % of the *Chlorobiales* reads. In general, we found a high number of unclassified lineages. The 20 most abundant ASV accounted for about 50 % of all sequences, twelve of those belonged to unclassified genera or

253 families (Figure S8B). The novelty was especially high within the *Chromatiaceae* five of
254 the eight ASV that ranked among the "top 20" belonged to an unclassified genus.

255

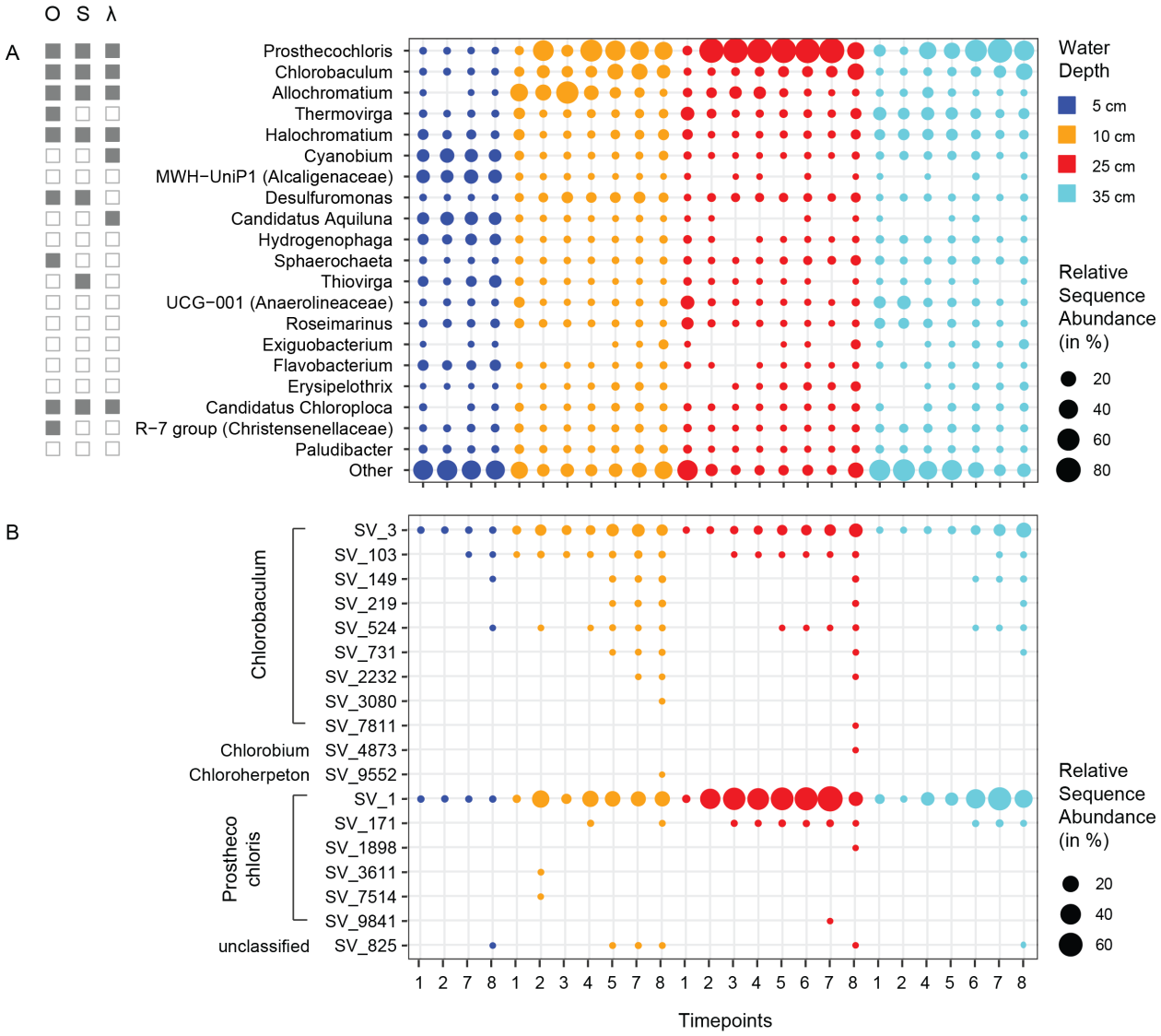

256

257 **Figure 6: Microbial community composition on genus level. A**: Relative sequence
258 abundance of genera found in different depths (colors) and timepoints (x-axis). Relative
259 sequence abundances were averaged across triplicates, due to the high similarity of all three
260 experiments. Clades that are anaerobic (O), involved in the sulfur cycle (S), or phototrophic (ƛ)
261 are indicated by full squares. **B**: Relative sequence abundance of amplicon sequence variants
262 (ASV) within the order *Chlorobiales*. The graph shows average values of the three replicate
263 experiments for clarity. The replicate experiments were very similar (see SI Figure S5 and S6).

264

Chlorobiales-affiliated metagenome-assembled genomes

We calculated the index of replication (iRep) (Brown et al., 2016) of the *Prosthecochloris* and *Chlorobaculum* populations based on the metagenome-assembled genomes (MAGs) that were recovered from the community metagenomes of two replicate experiments (Replicates A, E) and the enrichment culture (SK) at timepoint 7. Both populations were replicating rapidly. *Prosthecochloris* (bin10) had an iRep value of 3.7 (r^2=0.90, sample 7A3), which indicates that on average every cell had 2.5 replication events at the time of sampling. *Chlorobaculum* (bin 6) had iRep values of 2.5 (r^2=0.95, sample 7E3) and 2.8 (r^2=0.95, sample 7K3), indicating that on average every cell had ~1.5 replication events. Bin 6 (*Chlorobaculum sp.)* and Bin 10 (*Prosthecochloris sp.*) contain CRISPR arrays denoted as either type I (*cas3*) or III (*cas10*) CRISPR systems (Makarova et al., 2015) (Figure S16, S17). CRISPR predictions revealed 3 direct repeat sequences in both MAGs of 30 and 35 (2) bp in length for Bin 6 and 37, 32, and 33 for the Bin 10 (Table S4). None of the spacers were shared by the closest reference and representative genomes or matched sequences in the CRISPR database (Grissa et al., 2007). However, a highly similar CRISPR array and direct repeat sequence were found between our Bin 6 and *Chlorobaculum parvum* NCBI8327 with 60% *cas* genes similarity (Figure S16). The metagenomes of all experiments, as well as of the GSB enrichment culture contained high relative sequence abundances of viruses affiliating with *Microviridae* (Figure S18).

Discussion

In this study, we mimicked naturally-occurring disturbances in the decaying seagrass bed of Trunk River to study microbial community succession. We performed triplicate experiments that showed very similar physicochemical gradients and patterns of community structure. The observed slight variations between replicate sites were likely due to differences in the organic matter composition and distance to the lagoon access, or due to ripples and disturbances caused by weather, animals, and sampling scientists. The replicated disturbances of the organic matter layers (A-hole, E-hole, and K-hole) released trapped sulfide and caused the rapid establishment of steep physicochemical gradients as well as the development of a bloom of sulfide-oxidizing phototrophs. We

295 monitored the community assembly and succession and highlight the ecological niches
296 of key populations and their possible mechanisms of coexistence.

297 Biogeochemistry of the water column

298 The Trunk River lagoon is a brackish estuary approximately on sea level and
299 characterized by shallow, warm water. It has one small freshwater inlet, and one small
300 outlet to the sea, resulting in a long residence time and low flow velocity of the water.
301 The freshwater overlays a saltwater lens creating very a stable salinity gradient from
302 brackish water at the surface to basically seawater at the sediment surface in 40 cm
303 water depth (Figure 2), typical of brackish water estuaries (Levinton, 1995). Before the
304 experiment the pH decreased from mildly basic near the surface (~ pH 9) to around
305 seawater near the sediments (~ pH 8). After the disturbance the salinity gradient
306 remained stable over the 15-day sampling period, pH however decreased drastically in
307 all layers to as low as ~ 6.25 in the bottom layers (Figure 2). This pH decrease is likely
308 due to hydrogen sulfide and its dissociation from H_2S to HS^-. The dissolved oxygen
309 (DO) concentration also decreased with water depth (Figure 2) being below 20 %
310 saturation in the bottom layers throughout most of the experiment, thus the bottom layer
311 being *de facto* anoxic. In addition, DO decreased substantially even in the top layers in
312 the first half of the experiment, recovering in parallel to the slow collapse of the bloom.
313 The larger variations in pH and DO at 5 cm and 10 cm as compared to 25 cm and 35
314 cm indicate that the top layers were the more dynamic part of the water column.
315 Together, the observations – that were very similar in the replicate experiments - show
316 that after the system settled from the initial perturbations, it reached a stable state with
317 stable physicochemical gradients in the stratified water column.

318 Indications for a cryptic sulfur cycle in the water column

319 Sulfate concentrations in the bottom layers decreased substantially within the first days,
320 and were lowest in the bloom layer at 25 cm depth, where sulfate was almost entirely
321 depleted. We found sulfate-reducers affiliating with *Desulfobacteraceae* and
322 *Desulfobulbaceae* in the hypoxic layers of the bloom (Figure S8) likely producing sulfide
323 using either hydrogen or organic acids released from fermented organic matter layers.

The sulfide concentrations were highest at the upper boundary of the bloom at 10 cm water depth after the system stabilized around day 6 (Figure 2). This is unexpected since reduced sulfur species, especially hydrogen sulfide, are the electron donor for the green and purple phototrophs and thus should have been depleted in these layers. At the same time, we found an increased relative abundance of sulfur-reducing *Desulfuromonas sp.* in the bloom layers, peaking at around 15 % relative sequence abundance. *Desulfuromonas sp.* are known to live in freshwater ecosystems and reduce elemental sulfur to sulfide (Finster et al., 1997, 1994; Pfennig and Biebl, 1976), which in turn can be reused by the sulfide-oxidizing phototrophs. This suggests that sulfide was replenished by sulfate reducers from sulfate as well as from sulfur reducers from sulfur produced by the phototrophs indicating a “sulfur loop” in the bloom carried out by multiple species across several phyla (Figure 7). At early timepoints the microbial suspension was beige and milky, indicating the presence of large amounts of elemental sulfur in the sample (Figure S2). Later the samples turned more yellow, due to an increase in phototrophic organisms and their photopigments (Figure 2, 3), but also cleared up and became translucent (Figure S2). Taken together this indicates that *Desulfuromonas sp.* reduced the elemental sulfur that was produced by the anoxygenic phototrophs so quickly that it was not accumulating in the suspension. This suggested sulfur loop - potentially a cryptic sulfur cycle depending on the concentration of the intermediate S^0 - provides a positive feedback that could explain the very rapid development of the bloom. The involved *Chlorobi* and *Deltaproteobacteria* could even form tight aggregates to efficiently use the common intermediate similar to *Chlorochromatium aggregatum* (Wanner et al., 2008), a topic that merits future research.

Assembly and coexistence of phototrophic microorganisms

The yellowish layer in the water column (fondly termed “microbial lemonade”, Figure 1C) formed around two to four days post-disturbance and was fully established by day six. The lemonade layer occurred between 10 – 30 cm water depth (Figure S2) with highest cell numbers and biomass at around 25 cm water depth (Figure 2, S4) in brackish, mildly acidic, and hypoxic waters (Figure 2). The microbial lemonade

354 represented a multispecies phototrophic bloom, dominated by green and purple sulfur
355 bacteria. Due to the relative influence of green and purple sulfur bacteria and their
356 photopigments, the color of the bloom slightly shifted from yellow-green at early
357 timepoints to orange at mid timepoints back to yellow-green at late timepoints (Figure
358 S2). This is reflected by the pigment spectra collected at the different timepoints (Figure
359 3).

360 Interestingly, the sequencing data suggested that especially the lower layer of the
361 bloom was dominated by an apparently clonal population of green sulfur bacteria
362 affiliated with *Prosthecochloris vibrioformis*. The green sulfur bacteria are sulfur-
363 oxidizing, strictly anaerobic, obligate photoautotrophs (Alexander and Imhoff, 2006).
364 Yet, based on our oxygen measurements, the Trunk River GSB population apparently
365 tolerated low oxygen concentrations. The low concentration of dissolved oxygen at 25
366 cm depth combined with sulfide, salinity, and low light created an optimal habitat for
367 *Prosthecochloris sp*.

368 Despite the dominance of few populations the disturbance created a habitat with
369 gradients of pH, salinity, light, oxygen, and sulfide that enabled the coexistence of
370 multiple phototrophic clades from at least five different phyla (*Actinobacteria, Chlorobi,*
371 *Chloroflexi, Cyanobacteria and Gammaproteobacteria*). The coexistence of these high
372 number of organisms competing for the same energy source is due to the different
373 absorption maxima of each clades' photopigments (Figure 3), need for different electron
374 donors, and the varying salinity and oxygen tolerances of each clade. *P. vibrioformis* is
375 absent at 5 cm and present only in low abundance at 10 cm. The surface layer (5 cm
376 depth) is inhabited by oxygenic phototrophic *Cyanobacteria* affiliating with *Cyanobium*,
377 while the upper layer of the bloom (10 cm depth) is dominated by purple sulfur bacteria
378 of the order *Chromatiales* (Figure 6). Because *Prosthecochloris* are adapted to low light
379 conditions (Findlay et al., 2015) and respond to different wavelengths of light than
380 *Cyanobacteria* and photosynthetic *Proteobacteria* (Herbert and Tanner, 1977; Parkin
381 and Brock, 1980), it is reasonable that they thrived at depths of 25 cm, where they can
382 out-compete other phototrophs. *Prosthecochloris* have been previously observed in
383 many marine and saline habitats, such as the Black Sea (Manske et al., 2005), Baltic

Sea, Sippewissett Salt Marsh, and Badwater basin (Alexander and Imhoff, 2006). They are considered to belong to a specialized phylogenetic lineage of green sulfur bacteria adapted for marine and salt water ecosystems. Blooms of *P. vibrioformis* have been previously observed in stratified lakes, where they dominate the community at a specific depth (Máthé et al., 2014), sometimes forming clonal blooms (Gregersen et al., 2009).

Remarkably, the suspended phototrophic bloom was spatially organized analogous to benthic phototrophic mats in the nearby Sippewissett Salt Marsh (Armitage et al., 2012; Nicholson et al., 1987; Pierson et al., 1987) and elsewhere (Bolhuis et al., 2014; Bolhuis and Stal, 2011). The layers of phototrophic mats are dominated from top, middle to bottom by *Cyanobacteria*, PSB and GSB, respectively, except on a scale of few millimeters to centimeters. Thus, the disturbance experiment that we performed *in situ* created a transient ecosystem with niches resembling those in coastal microbial mats, except across a spatial scale that was one order of magnitude greater. The community slowly collapsed after about two weeks and the water column seemed to return to its original state (Figure 5). We did not observe a shift from phototrophic to chemotrophic sulfur oxidation after the phototrophic bloom (Pjevac et al., 2015).

New species of purple and green sulfur bacteria and possible viral predation

Due to the findings of a previous study based on 16S rRNA gene libraries, Imhoff and colleagues proposed the existence of several uncultivated GSB species in Sippewissett Salt Marsh and other estuaries (Alexander and Imhoff, 2006). The authors provide evidence that several GSB clades harbor species that have yet escaped isolation, among those are species in the genera *Chlorobaculum* and *Prosthecochloris*. We have strong evidence that we found at least two of these species based on our MAGs of a *Chlorobaculum* species (Bin 6, Figure S12, S14) and a *Prosthecochloris* species (Bin 10, Figure S12, S15). Both MAGs cluster sufficiently far away from the closest cultured species (Figure S11, S13) and have average nucleotide identity (ANI) values of <90 to their respective closest cultured isolate. Both MAGs also contain CRISPR-Cas systems that are very different from the cultured isolates (Figure S16, S17). Our CRISPR results show that Trunk River populations may be under predatory stress, affecting the abundance of bacterial blooms, and that host immunity is active in this ecosystem

(Llorens-Marès et al., 2017). The unique CRISPR arrays indicate that closely related species may be infected by different viruses with species specificity (Borton et al., 2018). However, some viral populations have been reported to have broad host ranges (Daly et al., 2019). Divergent evolution or strain level microdiversity may also explain distinct CRISPR-Cas systems (Daly et al., 2016). A lack of public databases containing viral sequences restricts the detection of viral-host interactions (Goodcare et al., 2018). While Llorens-Marès *et al.* (2017) characterized a potential green sulfur bacterial viral infection, to date, phages infecting *Chlorobi* have not been reported. Our analyses suggest that viruses of the family *Microviridae* played a major role in the transient bloom (Figure S17), possibly even for its demise. This interesting finding merits future research on transient phototrophic blooms in estuarine ecosystems.

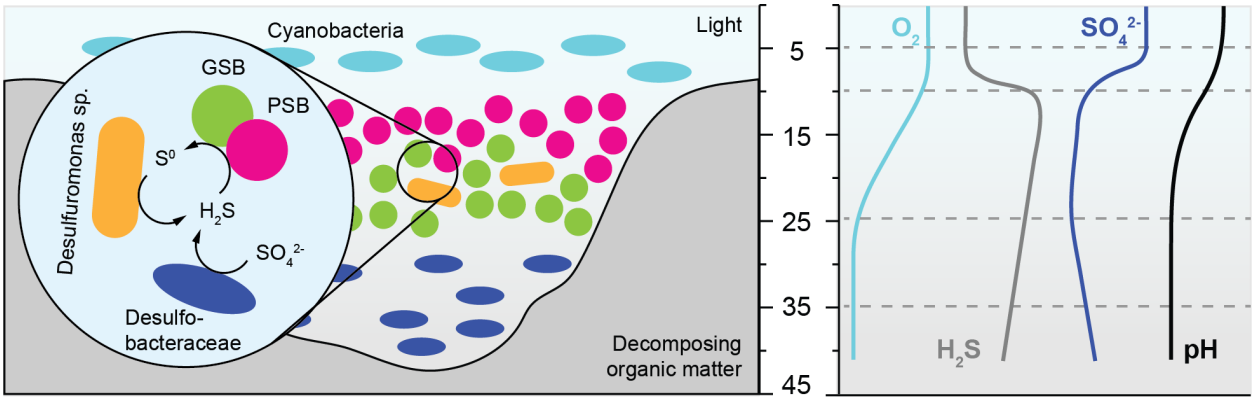

Figure 7: Ecosystem sketch. Schematic overview of the phototrophic bloom showing the main phototrophic populations, sulfur compounds, and chemical gradients.

Conclusions

In this study, we mimicked phototrophic blooms that naturally occur in a brackish estuarine ecosystem to understand the underlying microbial and biogeochemical dynamics. We suggest that phototrophs of different phyla co-exist in a layered bloom based on their different light and oxygen requirements, analogous to the communities in phototrophic microbial mats (Figure 7). Our findings indicate that Chlorobiaceae form a syntrophic relationship with Desulfuromonas sp. with elemental sulfur as intermediate.

437 We reconstructed metagenome assembled genomes of two uncultured green sulfur
438 bacteria, belonging to *Chlorobaculum* and *Prosthecochloris* and show that *Microviridae*
439 viruses played a role in the bloom, potentially infecting species within the *Chlorobiales*.

440

441 **Materials and Methods**

442 Experimental Setup and Sample Collection

443 We used custom-made sampling poles for long-term environmental monitoring of the
444 water column without disturbing the established gradients (LEMON; Figure 1B, C). The
445 sampling poles were placed in three replicate depressions (A-hole, E-hole, and K-hole)
446 that we dug into the thick layers of decaying organic matter (Figure 1A). In each of sites,
447 a sampling pole was placed such that the inlets sampled water at 5 cm, 10 cm, 25 cm,
448 and 35 cm depth below the surface (Figure 1B, C). Sampling poles were set up one day
449 after the holes were dug out and sampling began one day after set up (two days post
450 disturbance), to allow disturbed sediment to settle. Samples were collected over a 15-
451 day period during July-August 2015. For each sample, the first 5 ml were discarded,
452 followed by collection of 100 ml of water in several sterile tubes for further analyses
453 (Figure S2). The tubes were transported on ice to the laboratory and stored at 4˚C. All
454 sample collections were carried out between 4 pm and 6 pm.

455 Enrichment cultures

456 To enrich for GSB we used a defined saltwater medium (400g/l NaCl, 60g/l
457 $MgCl_2$*$6H_2O$, 3g/l CaC_{l2}*$2H_2O$, 10g/l KCl) buffered at pH 7.2 with 5 mM MOPS. The
458 medium contained 5 mM NH_4Cl as N source, 1mM K phosphate (pH 7.2) as P source,
459 70 mM $NaHCO_3$ as C source, 10 mM $Na_2S_2O_3$ as electron donor, 1 mM Na_2S as
460 reductant or electron donor, a multivitamin solution prepared at 1000× in 10 mM MOPS
461 at pH 7.2, and a trace metal solution prepared at 1000× in 20 mM HCl. Saltwater base,
462 MOPS, N- and P-source, and trace metals were autoclaved together in a Widdel
463 sparging flask, cooled under a stream of N_2/CO_2 (80%:20%) gas. C-source, electron
464 donors and vitamins were added from filter-sterilized stock solutions after cooling. The

medium was inoculated with biomass removed from *in situ* enrichments of GSB grown on glass slides using a 770 nm monochromatic LED. After inoculation, the bottle was kept in dark for 2-4 hours and then placed 5 cm away from a LED light source with the same specifications. After a visible sign of growth – green coloration – the culture was filtered through 0.2 µm filter and used for DNA extraction, similar to other samples.

Physicochemical Measurements

In-situ measurements of pH, temperature, dissolved oxygen, oxidation reduction potential (ORP), and ion selective electrode (ISE) were carried out with a multi-parameter probe equipped with a quarto probe (YSI Professional Series Model Pro). The probe was calibrated for pH with 4, 7, and 10 buffers and for dissolved oxygen using oxygen-saturated water and an anoxic solution of sodium ascorbate and sodium hydroxide. After each sample collection the probe was lowered into the water to each depth per site and after probe readings stabilized, the parameters were recorded.

To measure biomass and pigment spectra, up to 10 ml of the collected sample was filtered through a sterile Millipore filter (0.2 µm GTTP, 0.2 µm GNWP, or 0.22 µm GV). Filtrates were washed twice with ammonium acetate solutions with the same ionic strength as each depth. The filters were placed on aluminum foil, dried at 60°C overnight and subsequently weighed (Figure S3). A Spectral Evolution SR1900 spectrophotometer was used to measure the spectrum of the dried biomass on each filter with a scanning range of 350-1900 nm. The light source was a Dyonics 60 W lamp.

After sterile filtration, the filtrate was used to measure anion, cation, and organic acid concentrations using an ion chromatographer. The ion concentrations of samples were measured by diluting filtrate 1:10 with Millipore water to a total volume of 2 ml. The diluted samples were measured in triplicate using a ThermoFisher/Dionex ICS2100 equipped with an AS18 column using a 13 minute, 33 mM NaOH isocratic program to measure anions and a CS12A column using a 13 minute, 25 mM methane sulfonic acid isocratic program to measure cations. Samples for organic acid analysis were filtered through 0.2 µm filters and 900 µL of filtrate was added to 100 uL of 5 M H_2SO4 to

494 precipitate any compounds that might do so on the column. The samples were
495 centrifuged and the upper portion was removed for HPLC analysis. Samples were
496 analyzed on a BioRad Aminex HPX-87H column in isocratic elution mode with 5 mM
497 sulfuric acid.

498 Iron concentration was quantified using the ferrozine assay (Stookey, 1970). 4.5 ml
499 filtrate were added on site to 0.5 ml of 1 M HCl to prevent oxidation of any available
500 Fe(III). For Fe(II), 50 µl filtrate was added to 50 µl of 1M HCl and 100 µl of ferrozine
501 (0.1% [wt/vol] in 50% ammonium acetate) was added. For total iron, 50 µl filtrate was
502 added to 50 µl of 10% hydroxylamine hydrochloride in 1M HCl to reduce Fe(III) to Fe(II).
503 Samples were added to 100 µl of ferrozine. All samples were incubated for 15 min and
504 a filtrates Absorbances were read in triplicate at 560 nm using a Promega plate reader.
505 Ferrous ammonium sulfate was used as standard.

506 Sulfide concentrations were quantified using the Cline assay (Cline, 1969). 1.5 ml filtrate
507 were added on site to 500 µl of zinc acetate solution (91 mM) to prevent oxidation of the
508 sulfide. Cline reagent (N, N-dimethyl-p-phenylenediamine sulfate, H_2SO_4,
509 $NH_4Fe(SO_4)_2 \cdot 12$ H2O) was added, the samples were incubated in the dark for 30
510 minutes and absorbance was read at 665 nm.

511 DNA Extraction, Library Preparations, and Sequencing

512 Within 2 – 6 hours of sample collection, 50 ml sample was filtered using an autoclaved
513 0.2 µm polycarbonate filter (GTTP Millipore) and stored at -20˚C. Each filter was cut
514 with a sterile blade and extracted with the MoBio PowerFecal kit. We followed the
515 protocol, but instead of bead beating, the samples were twice vortexed horizontally with
516 the beads (10 min and 20 min with a 10 min pause). DNA concentration and purity were
517 measured with Nanodrop and Promega Qubit fluorometer and Nanodrop, respectively.

518 We prepared 16S rRNA gene amplicon library using V4-V5 fusion primers as previously
519 described (Morrison et al., 2013). Briefly, the fusion primer contains TruSeq adapter
520 sequences, barcodes, and the forward or reverse 16S rRNA gene primers. The forward
521 and reverse 16S rRNA gene primers were 518F (CCAGCAGCYGCGGTAAN) and 926R
522 (CCGTCAATTCNTTTRAGT). The PCR conditions were as follows: initial denaturation

of 94˚C for 3 min, 30 cycles of denaturation at 94˚C for 30 s, annealing at 57˚C for 45 s, extension at 72˚C for 1 min, and final extension at 72˚C for 2 min. The libraries were cleaned using Agencourt Ampure XP beads, quantified using picogreen, pooled in equimolar ratios, and cleaned again using Agencourt Ampure XP beads a second time. The indexed libraries were then sequenced on the Illumina MiSeq PE250 platform.

The DNA from the depth of 25 cm from timepoint 7 from the three replicates, as well as from a phototrophic enrichment were used to generate whole-genome shotgun metagenomic library. The DNA was sheered using Covaris sonicator, size selected for 500-600bp using Pippin prep, and cleaned using Agencourt Ampure XP clean beads. The cleaned DNA was analyzed using Bioanalyzer DNA1000 chip and amplified using random hexamer primers with KAPA polymerase for 10-12 cycles. Amplified DNA was cleaned using Agencourt Ampure XP clean beads and used to prepare metagenomic library using Nugen Ovation ultralow DR multiplex kit with manufacture supplied protocol. The libraries were then sequenced on Illumina MiSeq PE250 platform. All the sequencing was performed at the Keck facility at the J. Bay Paul Center at the Marine Biological Laboratory, Woods Hole, MA.

Amplicon Sequence Data Analyses

The amplicon data was demultiplexed in mothur v1.39.5 (Schloss et al., 2009), followed by the trimming of 16S rRNA gene amplification primers using Cutadapt v1.16 (Martin, 2011) with default parameters. The primer-trimmed amplicon sequencing data was quality checked using DADA2 v1.9.0 R Package (Callahan et al., 2016). In DADA2, the reads were trimmed at the first instance of quality drop below 8, an expected error rate of 2, followed by trimming to 220bp and 200bp for forward and reverse reads. Any reads that matched PhiX or had an ambiguous base were removed. An error profile for the forward and reverse reads was generated using learnErrors function and then used to merge the forward and reverse reads using the mergePairs function. The merged reads were used to generate the amplicon sequence variants using makeSequenceTable function, which was then filtered for chimeras using removeBimeraDenovo function. The amplicon sequence variants were assigned taxonomy in DADA2 using Silva reference database v132 (Quast et al., 2013). Community analyses were performed using a

custom workflow based on R and the packages vegan, labdsv, tidyverse (stringr, dplyr, ggplot2), UpSetR and custom scripts (Conway et al., 2017; Oksanen et al., 2012; Roberts, 2012; Wickham, 2018, 2009; Wickham et al., 2018) for details see. Relative abundance of bacterial ASV (amplicon sequence variants), Bray-Curtis dissimilarities, Nonmetric Multidimensional Scaling as well as analyses determining Singletons and percent shared ASVs are based on the unaltered Sample×ASV table as calculated by DADA2. To compare the diversity between samples using the number of observed species, Shannon index, Inverse Simpson diversity and Chao1 Richness (Hill et al., 2003) the ASV abundance tables were rarefied to account for unequal sampling effort using 31,682 randomly chosen sequences without replacement. For details refer to the R workflow available at the public database PANGAEA (https://issues.pangaea.de/browse/PDI-20394). Note: This link is inactive until the submitted data are processed and public.

Metagenomic Sequence Data Analyses

Quality control of the raw reads was performed using Preprocessing and Information of SEQuence data (PRINSEQ) to remove sequencing tags and sequences with mean quality score lower than 25, duplicates and N's (Schmieder and Edwards, 2011). All runs combined provided a total of approximately 3.5 million 250 bp read pairs. All forward and reverse reads were placed together in one file and cross co-assembled using SPAdes using the --meta option (Bankevich et al., 2012). Binning was performed using MetaBAT (Kang et al., 2015) and Anvi'o (v5.2) metagenomic workflow (CONCOCT) (Eren et al., 2015). Completeness and contamination of bins was assessed using CheckM (Parks et al., 2015). Assembled genomes that contained more than 90% genome completeness, less than 5% contamination, and sequences mainly from a single genus were further analyzed. This yielded two high quality bacterial metagenome-assembled genomes (MAGs): Bin 6 and Bin 10. Taxonomic composition for each bin was predicted using FOCUS (Silva et al., 2014). Phylogenetic analysis including the identification of their closest phylogenetic neighbors was investigated using PATRIC Comprehensive Genome Analysis (Wattam et al., 2017). CRISPRCasFinder (Couvin et al., 2018) and CRISPRone (Zhang and Ye, 2017) were

used to identify CRISPR repeat and spacer sequences. The quality checked reads from each sample were mapped to the MAGs, Bin 6 and Bin 10 using bowtie2 (Langmead and Salzberg, 2012). The mapped reads were then analyzed using iRep (Brown et al., 2016) to estimate replication events in Bin 6 and Bin 10. Unassembled sequences were processed on the MG-RAST platform version 4.0.3. Percent abundance of viral sequences was calculated from the RefSeq database using an e-value cutoff of 1e-5, a minimum identity cutoff of 60%, and an alignment length minimum cutoff of 15 (Meyer et al., 2008). For details refer to the metagenome analyses workflow publicly accessible at HackMD (https://hackmd.io/tGZyCM9sSNmuorpHenQVNA).

Availability of data and material

The genomic datasets generated and analyzed during the current study are available on MG-RAST (Project Name: Trunk River, ID: 4837589.3 (sample SK), 4837590.3 (sample 7K3), 4837591.3 (sample 7E3), 4837592.3 (sample 7A3)) and metagenome-assembled genomes workflow are available on HackMD (https://hackmd.io/tGZyCM9sSNmuorpHenQVNA). The raw 16S rRNA amplicon data, the shotgun metagenomic data, the 16S rRNA gene clonal sequences, and the metagenome assembled genomes presented in this work are publicly archived in NCBI under Bioproject PRJNA530984 (https://www.ncbi.nlm.nih.gov/bioproject/530984). The contextual datasets generated and analyzed during the current study are publicly available at PANGAEA under accession XXX (weblink).

Funding

This work was carried out at the Microbial Diversity summer course at the Marine Biological Laboratory in Woods Hole, MA. The course was supported by grants from National Aeronautics and Space Administration, the US Department of Energy, the Simons Foundation, the Beckman Foundation, and the Agouron Institute.

Competing interests

The authors declare that they have no competing interests.

Authors' contributions

SB helped design the study, collected samples, prepared and analyzed sequencing data, wrote manuscript

ESC helped design the study, collected samples, prepared and analyzed physicochemical data, wrote manuscript

SHK helped design the study and enrichment cultures, analyzed physicochemical data and pigment spectra, wrote manuscript

SPC analyzed metagenomic data, wrote manuscript

SK obtained enrichment culture, wrote manuscript

SD helped design the study, wrote manuscript

KH collected samples, prepared and analyzed physicochemical data and pigment spectra, wrote manuscript

SER designed the study, analyzed and visualized sequencing and physicochemical data, wrote manuscript with input from all co-authors

All authors read and approved the final manuscript.

Acknowledgements

We would like to express our deepest gratitude towards Dianne Newman and Jared R. Leadbetter, directors of the Microbial Diversity Summer Course at the Marine Biological Laboratory 2014-2017. Without their trust, support and encouragement the project would not have been realized. We are very grateful to Joseph Vinneis, Kim Finnegan, and Mitchell Sogin for providing laboratory space, equipment, and guidance regarding next-generation sequencing. We are also very grateful to the students and staff of the 2015 Microbial Diversity Summer Course, specifically Kurt Dahlstrom, Kristina Garcia, Jessica Choi, Rachel Soble, and Lina Bird. We would like to thank the Simons Foundation, NSF, DOE, and NASA for funding the Microbial Diversity Summer course,

as well as Promega, Thermo Fisher Scientific, Spectral Evolution, and MBL's Marine Resources Center for providing reagents and equipment used in this work.

References

Alexander B, Imhoff JF. 2006. Communities of green sulfur bacteria in marine and saline habitats analyzed by gene sequences of 16S rRNA and Fenna-Matthews-Olson protein. *Int Microbiol* **9**:259–266.

Allen GP, Salomon JC, Bassoullet P, Du Penhoat Y, de Grandpré C. 1980. Effects of tides on mixing and suspended sediment transport in macrotidal estuaries. *Sediment Geol* **26**:69–90. doi:10.1016/0037-0738(80)90006-8

Armitage DW, Gallagher KL, Youngblut ND, Buckley DH, Zinder SH. 2012. Millimeter-scale patterns of phylogenetic and trait diversity in a salt marsh microbial mat. *Front Microbiol* **3**:293. doi:10.3389/fmicb.2012.00293

Badr E-SA, Tappin AD, Achterberg EP. 2008. Distributions and seasonal variability of dissolved organic nitrogen in two estuaries in SW England. *Mar Chem* **110**:153–164. doi:http://dx.doi.org/10.1016/j.marchem.2008.04.007

Bankevich A, Nurk S, Antipov D, Gurevich A a., Dvorkin M, Kulikov AS, Lesin VM, Nikolenko SI, Pham S, Prjibelski AD, Pyshkin A V., Sirotkin A V., Vyahhi N, Tesler G, Alekseyev M a., Pevzner P a. 2012. SPAdes: A New Genome Assembly Algorithm and Its Applications to Single-Cell Sequencing. *J Comput Biol* **19**:455–477. doi:10.1089/cmb.2012.0021

Bernhard AE, Colbert D, McManus J, Field KG. 2005. Microbial community dynamics based on 16S rRNA gene profiles in a Pacific Northwest estuary and its tributaries. *FEMS Microbiol Ecol* **52**:115–128. doi:10.1016/j.femsec.2004.10.016

Bolhuis H, Cretoiu MS, Stal LJ. 2014. Molecular ecology of microbial mats. *FEMS Microbiol Ecol* **90**:335–350. doi:10.1111/1574-6941.12408

Bolhuis H, Stal LJ. 2011. Analysis of bacterial and archaeal diversity in coastal microbial mats using massive parallel 16S rRNA gene tag sequencing. *ISME J* **5**:1701–1712.

Borrego CM, Gerola PD, Miller M, Cox RP. 1999. Light intensity effects on pigment composition and organisation in the green sulfur bacterium Chlorobium tepidum. *Photosynth Res* **59**:159–166. doi:10.1023/A:1006161302838

Borton MA, Daly RA, O'Banion B, Hoyt DW, Marcus DN, Welch S, Hastings SS, Meulia T, Wolfe RA, Booker AE, Sharma S, Cole DR, Wunch K, Moore JD, Darrah TH, Wilkins MJ, Wrighton KC. 2018. Comparative genomics and physiology of the genus *Methanohalophilus* , a prevalent methanogen in hydraulically fractured

671 shale. *Environ Microbiol* **20**:4596–4611. doi:10.1111/1462-2920.14467

672 Boschker HTS, Vasquez-Cardenas D, Bolhuis H, Moerdijk-Poortvliet TWC, Moodley L.
673 2014. Chemoautotrophic Carbon Fixation Rates and Active Bacterial Communities
674 in Intertidal Marine Sediments. *PLoS One* **9**:e101443.
675 doi:10.1371/journal.pone.0101443

676 Brown CT, Olm MR, Thomas BC, Banfield JF. 2016. Measurement of bacterial
677 replication rates in microbial communities. *Nat Biotechnol* **34**:1256–1263.
678 doi:10.1038/nbt.3704

679 Callahan BJ, McMurdie PJ, Rosen MJ, Han AW, Johnson AJA, Holmes SP. 2016.
680 DADA2: High-resolution sample inference from Illumina amplicon data. *Nat*
681 *Methods* **13**:581–583.

682 Capone DG, Kiene RP. 1988. Comparison of microbial dynamics in marine and
683 freshwater sediments: contrasts in anaerobic carbon catabolism. *Limnol Oceanogr*
684 **33**:725–749.

685 Caumette P, Imhoff JF, Süling J, Matheron R. 1997. Chromatium glycolicum sp. nov., a
686 moderately halophilic purple sulfur bacterium that uses glycolate as substrate. *Arch*
687 *Microbiol* **167**:11–18. doi:10.1007/s002030050410

688 Cline JD. 1969. Spectrophotometric determination of hydrogen sulfide in natural waters.
689 *Limnol Oceanogr* **14**:454–458.

690 Conway JR, Lex A, Gehlenborg N. 2017. UpSetR: An R Package For The Visualization
691 Of Intersecting Sets And Their Properties. *bioRxiv*.

692 Couvin D, Bernheim A, Toffano-Nioche C, Touchon M, Michalik J, Néron B, Rocha
693 EPC, Vergnaud G, Gautheret D, Pourcel C. 2018. CRISPRCasFinder, an update of
694 CRISRFinder, includes a portable version, enhanced performance and integrates
695 search for Cas proteins. *Nucleic Acids Res* **46**:W246–W251.
696 doi:10.1093/nar/gky425

697 Daly RA, Borton MA, Wilkins MJ, Hoyt DW, Kountz DJ, Wolfe RA, Welch SA, Marcus
698 DN, Trexler R V, MacRae JD, Krzycki JA, Cole DR, Mouser PJ, Wrighton KC.
699 2016. Microbial metabolisms in a 2.5-km-deep ecosystem created by hydraulic
700 fracturing in shales. *Nat Microbiol* **1**:16146.

701 Daly RA, Roux S, Borton MA, Morgan DM, Johnston MD, Booker AE, Hoyt DW, Meulia
702 T, Wolfe RA, Hanson AJ, Mouser PJ, Moore JD, Wunch K, Sullivan MB, Wrighton
703 KC, Wilkins MJ. 2019. Viruses control dominant bacteria colonizing the terrestrial
704 deep biosphere after hydraulic fracturing. *Nat Microbiol* **4**:352–361.
705 doi:10.1038/s41564-018-0312-6

706 Eren AM, Esen ÖC, Quince C, Vineis JH, Morrison HG, Sogin ML, Delmont TO. 2015.
707 Anvi'o: an advanced analysis and visualization platform for 'omics data. *PeerJ*
708 **3**:e1319. doi:10.7717/peerj.1319

709 Findlay AJ, Bennett AJ, Hanson TE, Luther GW. 2015. Light-Dependent Sulfide
710 Oxidation in the Anoxic Zone of the Chesapeake Bay Can Be Explained by Small
711 Populations of Phototrophic Bacteria. *Appl Environ Microbiol* **81**:7560–7569.
712 doi:10.1128/aem.02062-15

713 Finster K, Bak F, Pfennig N. 1994. Desulfuromonas acetexigens sp. nov., a
714 dissimilatory sulfur-reducing eubacterium from anoxic freshwater sediments. *Arch*
715 *Microbiol* **161**:328–332. doi:10.1007/BF00303588

716 Finster K, Coates JD, Liesack W, Pfennig4 N. 1997. Desulfuromonas thiophila sp. nov.,
717 a New Obligately Sulfur-Reducing Bacterium from Anoxic Freshwater Sediment. *Int*
718 *J Syst Bacteriol* 754–758. doi:10.1099/00207713-47-3-754

719 Garvine RW. 1985. A simple model of estuarine subtidal fluctuations forced by local and
720 remote wind stress. *J Geophys Res* **90**:11945–11948.
721 doi:10.1029/JC090iC06p11945

722 Goodcare N, Aljanahi A, Nandakumar S, Mikailov M, Khan AS. 2018. A Reference Viral
723 Database (RVDB) To Enhance Bioinformatics Analysis of High-Throughput
724 Sequencing for Novel Virus Detection. *mSphere* **3**:1–18.
725 doi:10.1128/mspheredirect.00069-18

726 Gregersen LH, Habicht KS, Peduzzi S, Tonolla M, Canfield DE, Miller M, Cox RP,
727 Frigaard N-U. 2009. Dominance of a clonal green sulfur bacterial population in a
728 stratified lake. *FEMS Microbiol Ecol* **70**:30–41. doi:10.1111/j.1574-
729 6941.2009.00737.x

730 Grissa I, Vergnaud G, Pourcel C. 2007. The CRISPRdb database and tools to display
731 CRISPRs and to generate dictionaries of spacers and repeats. *BMC Bioinformatics*
732 **8**:1–10. doi:10.1186/1471-2105-8-172

733 Haas LW. 1977. The effect of the spring-neap tidal cycle on the vertical salinity structure
734 of the James, York and Rappahannock Rivers, Virginia, U.S.A. *Estuar Coast Mar*
735 *Sci* **5**:485–496. doi:http://dx.doi.org/10.1016/0302-3524(77)90096-2

736 Henriques IS, Alves A, Tacão M, Almeida A, Cunha Â, Correia A. 2006. Seasonal and
737 spatial variability of free-living bacterial community composition along an estuarine
738 gradient (Ria de Aveiro, Portugal). *Estuar Coast Shelf Sci* **68**:139–148.
739 doi:http://dx.doi.org/10.1016/j.ecss.2006.01.015

740 Herbert RA, Tanner AC. 1977. The Isolation and Some Characteristics of
741 Photosynthetic Bacteria (Chromatiaceae and Chlorobiaceae) from Antarctic Marine
742 Sediments. *J Appl Bacteriol* **43**:437–445. doi:10.1111/j.1365-2672.1977.tb00770.x

743 Hill TCJ, Walsh KA, Harris JA, Moffett BF. 2003. Using ecological diversity measures
744 with bacterial communities. *FEMS Microbiol Ecol* **43**:1–11.

745 Jay DA, Orton PM, Chisholm T, Wilson DJ, Fain AM V. 2007. Particle trapping in
746 stratified estuaries: Application to observations. *Estuaries and Coasts* **30**:1106–

1125. doi:10.1007/BF02841400

Jørgensen BB, Revsbech NP. 1983. Colorless Sulfur Bacteria, Beggiatoa spp. and Thiovulum spp., in O2 and H2S Microgradients. *Appl Environ Microbiol* **45**:1261–1270.

Kang DD, Froula J, Egan R, Wang Z. 2015. MetaBAT, an efficient tool for accurately reconstructing single genomes from complex microbial communities. *PeerJ* **3**:e1165. doi:10.7717/peerj.1165

Langmead B, Salzberg SL. 2012. Fast gapped-read alignment with Bowtie 2. *Nat Methods* **9**:357.

Lee DY, Owens MS, Doherty M, Eggleston EM, Hewson I, Crump BC, Cornwell JC. 2015. The Effects of Oxygen Transition on Community Respiration and Potential Chemoautotrophic Production in a Seasonally Stratified Anoxic Estuary. *Estuaries and Coasts* **38**:104–117. doi:10.1007/s12237-014-9803-8

Levinton JS. 1995. Marine biology: function, biodiversity, ecology. Oxford University Press New York.

Llorens-Marès T, Liu Z, Allen LZ, Rusch DB, Craig MT, Dupont CL, Bryant DA, Casamayor EO. 2017. Speciation and ecological success in dimly lit waters: Horizontal gene transfer in a green sulfur bacteria bloom unveiled by metagenomic assembly. *ISME J* **11**:201–211. doi:10.1038/ismej.2016.93

Long RR. 1976. Mass and salt transfers and halocline depths in an estuary. *Tellus* **28**:460–472. doi:10.1111/j.2153-3490.1976.tb00695.x

Lv X, Ma B, Yu J, Chang SX, Xu J, Li Y, Wang G, Han G, Bo G, Chu X. 2016. Bacterial community structure and function shift along a successional series of tidal flats in the Yellow River Delta. *Sci Rep* **6**:36550. doi:10.1038/srep36550 https://www.nature.com/articles/srep36550#supplementary-information

Maie N, Boyer JN, Yang C, Jaffé R. 2006. Spatial, geomorphological, and seasonal variability of CDOM in estuaries of the Florida Coastal Everglades. *Hydrobiologia* **569**:135–150. doi:10.1007/s10750-006-0128-x

Makarova KS, Wolf YI, Alkhnbashi OS, Costa F, Shah SA, Saunders SJ, Barrangou R, Brouns SJJ, Charpentier E, Haft DH, Horvath P, Moineau S, Mojica FJM, Terns RM, Terns MP, White MF, Yakunin AF, Garrett RA, Van Der Oost J, Backofen R, Koonin E V. 2015. An updated evolutionary classification of CRISPR-Cas systems. *Nat Rev Microbiol* **13**:722–736. doi:10.1038/nrmicro3569

Manske AK, Glaeser J, Kuypers MMM, Overmann J. 2005. Physiology and Phylogeny of Green Sulfur Bacteria Forming a Monospecific Phototrophic Assemblage at a Depth of 100 Meters in the Black Sea. *Appl Environ Microbiol* **71**:8049–8060. doi:10.1128/aem.71.12.8049-8060.2005

Martin M. 2011. Cutadapt removes adapter sequences from high-throughput

785 sequencing reads. *EMBnet.journal* **17**:10. doi:10.14806/ej.17.1.200

786 Máthé I, Borsodi AK, Tóth EM, Felföldi T, Jurecska L, Krett G, Kelemen Z, Elekes E,
787 Barkács K, Márialigeti K. 2014. Vertical physico-chemical gradients with distinct
788 microbial communities in the hypersaline and heliothermal Lake Ursu (Sovata,
789 Romania). *Extremophiles* **18**:501–514. doi:10.1007/s00792-014-0633-1

790 McLusky DS, Elliott M. 2004. The estuarine ecosystem: ecology, threats and
791 management. Oxford University Press on Demand.
792 doi:10.1093/acprof:oso/9780198525080.001.0001

793 Meyer F, Paarmann D, D'Souza M, Olson R, Glass EM, Kubal M, Paczian T, Rodriguez
794 A, Stevens R, Wilke A, Wilkening J, Edwards RA. 2008. The metagenomics RAST
795 server – a public resource for the automatic phylogenetic and functional analysis of
796 metagenomes. *BMC Bioinformatics* **9**:1–8. doi:10.1186/1471-2105-9-386

797 Møller MM, Nielsen LP, Jørgensen BB. 1985. Oxygen Responses and Mat Formation
798 by Beggiatoa spp. *Appl Environ Microbiol* **50**:373–382.

799 Moore WS. 1999. The subterranean estuary: a reaction zone of ground water and sea
800 water. *Mar Chem* **65**:111–125. doi:http://dx.doi.org/10.1016/S0304-4203(99)00014-
801 6

802 Moran MA, Sheldon WM, Zepp RG. 2000. Carbon loss and optical property changes
803 during long-term photochemical and biological degradation of estuarine dissolved
804 organic matter. *Limnol Oceanogr* **45**:1254–1264. doi:10.4319/lo.2000.45.6.1254

805 Morrison HG, Grim SL, Vineis JH, Mitchell LS. 2013. 16S amplicon fusion primers and
806 protocol for Illumina platform sequencing. doi:10.6084/m9.figshare.833944.v1

807 Muylaert K, Sabbe K, Vyverman W. 2000. Spatial and Temporal Dynamics of
808 Phytoplankton Communities in a Freshwater Tidal Estuary (Schelde, Belgium).
809 *Estuar Coast Shelf Sci* **50**:673–687. doi:http://dx.doi.org/10.1006/ecss.2000.0590

810 Nelson JL, Zavaleta ES. 2012. Salt Marsh as a Coastal Filter for the Oceans: Changes
811 in Function with Experimental Increases in Nitrogen Loading and Sea-Level Rise.
812 *PLoS One* **7**:e38558. doi:10.1371/journal.pone.0038558

813 Nicholson JAM, Stolz JF, Pierson BK. 1987. Structure of a microbiol mat at Great
814 Sippewissett Marsh, Cape Cod, Massachusetts. *FEMS Microbiol Lett* **45**:343–364.
815 doi:10.1016/0378-1097(87)90021-8

816 Oksanen J, Blanchet FG, Kindt R, Legendre P, Minchin PR, O´Hara RB, Simpson GL,
817 Solymos P, Stevens MHH, Wagner H. 2012. vegan: Community Ecology Package.

818 Oren A. 2011. Characterization of Pigments of Prokaryotes and Their Use in Taxonomy
819 and Classification. *Methods Microbiol* **38**:261–282. doi:10.1016/B978-0-12-387730-
820 7.00012-7

821 Pant HK, Reddy KR. 2001. Phosphorus Sorption Characteristics of Estuarine

822 Sediments under Different Redox Conditions. *J Environ Qual* **30**:1474.
823 doi:10.2134/jeq2001.3041474x

824 Parkin TB, Brock TD. 1980. The effects of light quality on the growth of phototrophic
825 bacteria in lakes. *Arch Microbiol* **125**:19–27. doi:10.1007/bf00403193

826 Parks DH, Imelfort M, Skennerton CT, Hugenholtz P, Tyson GW. 2015. CheckM:
827 assessing the quality of microbial genomes recovered from isolates, single cells,
828 and metagenomes. *Genome Res* **25**:1043–1055. doi:10.1101/gr.186072.114

829 Peduzzi P, Herndl GJ. 1991. Decomposition and significance of seagrass leaf litter
830 (Cymodocea nodosa) for the microbial food web in coastal waters (Gulf of Trieste,
831 Northern Adriatic Sea). *Mar Ecol Prog Ser* **71**:163–174.

832 Pfennig N, Biebl H. 1976. Desulfuromonas acetoxidans gen. nov. and sp. nov., a new
833 anaerobic, sulfur-reducing, acetate-oxidizing bacterium. *Arch Microbiol* **110**:3–12.
834 doi:10.1007/BF00416962

835 Pierson B, Oesterle A, Murphy GL. 1987. Pigments, light penetration, and
836 photosynthetic activity in the multi-layered microbial mats of Great Sippewissett
837 Salt Marsh, Massachusetts. *FEMS Microbiol Lett* **45**:365–376. doi:10.1016/0378-
838 1097(87)90022-X

839 Pjevac P, Korlević M, Berg JS, Bura-Nakić E, Ciglenečki I, Amann R, Orlić S. 2015.
840 Community shift from phototrophic to chemotrophic sulfide oxidation following
841 anoxic holomixis in a stratified seawater lake. *Appl Environ Microbiol* **81**:298–308.
842 doi:10.1128/AEM.02435-14

843 Purdy KJ, Embley TM, Nedwell DB. 2002. The distribution and activity of sulphate
844 reducing bacteria in estuarine and coastal marine sediments. *Antonie Van*
845 *Leeuwenhoek* **81**:181–187. doi:10.1023/a:1020550215012

846 Quast C, Pruesse E, Yilmaz P, Gerken J, Schweer T, Yarza P, Peplies J, Glöckner FO.
847 2013. The SILVA ribosomal RNA gene database project: improved data processing
848 and web-based tools. *Nucleic Acids Res* **41**:D590–D596. doi:10.1093/nar/gks1219

849 Ritchie AE, Johnson ZI. 2012. Abundance and Genetic Diversity of Aerobic Anoxygenic
850 Phototrophic Bacteria of Coastal Regions of the Pacific Ocean. *Appl Environ*
851 *Microbiol* **78**:2858–2866. doi:10.1128/aem.06268-11

852 Roberts DW. 2012. labdsv: Ordination and Multivariate Analysis for Ecology.

853 Schloss PD, Westcott SL, Ryabin T, Hall JR, Hartmann M, Hollister EB, Lesniewski RA,
854 Oakley BB, Parks DH, Robinson CJ, Sahl JW, Stres B, Thallinger GG, Van Horn
855 DJ, Weber CF. 2009. Introducing mothur: Open-source, platform-independent,
856 community-supported software for describing and comparing microbial
857 communities. *Appl Environ Microbiol* **75**:7537–7541. doi:10.1128/AEM.01541-09

858 Schmieder R, Edwards R. 2011. Quality control and preprocessing of metagenomic
859 datasets. *Bioinformatics* **27**:863–4. doi:10.1093/bioinformatics/btr026

Silva GGZ, Cuevas D a, Dutilh BE, Edwards R a. 2014. FOCUS: an alignment-free model to identify organisms in metagenomes using non-negative least squares. *PeerJ* **2**:e425. doi:10.7717/peerj.425

Simpson JH, Brown J, Matthews J, Allen G. 1990. Tidal straining, density currents, and stirring in the control of estuarine stratification. *Estuaries* **13**:125–132. doi:10.2307/1351581

Smith S V, Hollibaugh JT. 1993. Coastal metabolism and the oceanic organic carbon balance. *Rev Geophys* **31**:75–89. doi:10.1029/92RG02584

Srinivas TNR, Anil Kumar P, Sucharitha K, Sasikala C, Ramana C V. 2009. Allochromatium phaeobacterium sp. nov. *Int J Syst Evol Microbiol* **59**:750–753. doi:10.1099/ijs.0.65647-0

Stomp M, van Dijk MA, van Overzee HMJ, Wortel MT, Sigon CAM, Egas M, Hoogveld H, Gons HJ, Huisman J. 2008. The timescale of phenotypic plasticity and its impact on competition in fluctuating environments. *Am Nat* **172**:169–85. doi:10.1086/591680

Stookey LL. 1970. Ferrozine---a new spectrophotometric reagent for iron. *Anal Chem* **42**:779–781. doi:10.1021/ac60289a016

Waidner LA, Kirchman DL. 2005. Aerobic anoxygenic photosynthesis genes and operons in uncultured bacteria in the Delaware River. *Environ Microbiol* **7**:1896–1908.

Wanner G, Vogl K, Overmann J. 2008. Ultrastructural characterization of the prokaryotic symbiosis in "Chlorochromatium aggregatum". *J Bacteriol* **190**:3721–30. doi:10.1128/JB.00027-08

Wattam AR, Davis JJ, Assaf R, Boisvert S, Brettin T, Bun C, Conrad N, Dietrich EM, Disz T, Gabbard JL, Gerdes S, Henry CS, Kenyon RW, Machi D, Mao C, Nordberg EK, Olsen GJ, Murphy-Olson DE, Olson R, Overbeek R, Parrello B, Pusch GD, Shukla M, Vonstein V, Warren A, Xia F, Yoo H, Stevens RL. 2017. Improvements to PATRIC, the all-bacterial bioinformatics database and analysis resource center. *Nucleic Acids Res* **45**:D535–D542. doi:10.1093/nar/gkw1017

Wickham H. 2018. stringr: Simple, Consistent Wrappers for Common String Operations.

Wickham H. 2009. ggplot2: Elegant Graphics for Data Analysis. New York: Springer-Verlag New York.

Wickham H, François R, Henry L, Müller K. 2018. dplyr: A Grammar of Data Manipulation.

Wimpenny JWT, Wiegel J, Kuenen JG. 1982. Responses of Microorganisms to Physical and Chemical Gradients [and Discussion]. *Philos Trans R Soc Lond B Biol Sci* **297**:497–515.

Zaikova E, Walsh DA, Stilwell CP, Mohn WW, Tortell PD, Hallam SJ. 2010. Microbial community dynamics in a seasonally anoxic fjord: Saanich Inlet, British Columbia. *Environ Microbiol* **12**:172–191. doi:10.1111/j.1462-2920.2009.02058.x

Zhang Q, Ye Y. 2017. Not all predicted CRISPR–Cas systems are equal: isolated cas genes and classes of CRISPR like elements. *BMC Bioinformatics* **18**:92. doi:10.1186/s12859-017-1512-4

Zopfi J, Ferdelman TG, Jørgensen BB, Teske A, Thamdrup B. 2001. Influence of water column dynamics on sulfide oxidation and other major biogeochemical processes in the chemocline of Mariager Fjord (Denmark). *Mar Chem* **74**:29–51. doi:http://dx.doi.org/10.1016/S0304-4203(00)00091-8